Reaching 90% photoluminescence quantum yield in one-dimensional metal halide $C_4N_2H_{14}PbBr_4$ by pressure-suppressed non-radiative loss

Yingqi Wang[1†], Songhao Guo[1], Hui Luo[1], Chenkun Zhou[2‡], Haoran Lin[3§], Xuedan Ma[4], Qingyang Hu[1], Mao-hua Du[5], Biwu Ma[2,3*], Wenge Yang[1*], and Xujie Lü[1*]

[1]Center for High Pressure Science & Technology Advanced Research, Shanghai 201203, China.

[2]Department of Chemical and Biomedical Engineering, FAMU-FSU College of Engineering, Florida State University, Tallahassee, FL 32310, USA.

[3]Department of Chemistry and Biochemistry, Florida State University, Tallahassee, FL 32306, USA.

[4]Center for Nanoscale Materials, Argonne National Laboratory, Lemont, IL 60439, USA.

[5]Materials Science and Technology Division, Oak Ridge National Laboratory, Oak Ridge, TN 37831, USA.

KEYWORDS: low-dimensional hybrid metal halide, high pressure, self-trapped excitons, enhanced photoluminescence quantum yield, PL lifetime, non-radiative recombination.

ABSTRACT: Low-dimensional perovskite-related metal halides have emerged as a new class of light-emitting materials with tunable broadband emission from self-trapped excitons (STEs). Although various types of low-dimensional structures have been developed, fundamental understating of the structure-property relationships for this class of materials is still very limited, and further improvement of their optical properties remains greatly important. Here, we report a significant pressure-induced photoluminescence (PL) enhancement in a one-dimensional hybrid metal halide $C_4N_2H_{14}PbBr_4$ and the underlying mechanisms are investigated using *in situ* experimental characterization and first-principles calculations. Under a gigapascal pressure scale, the PL quantum yields (PLQYs) were quantitatively determined to show a dramatic increase from the initial value of 20% at ambient conditions to over 90% at 2.8 GPa. With *in situ* characterization of photophysical properties and theoretical analysis, we found that the PLQY enhancement was mainly attributed to the greatly suppressed non-radiative decay. Pressure can effectively tune the energy level of self-trapped states and increase the exciton binding energy, leading to a larger Stokes shift. The resulting highly-localized excitons with stronger binding reduce the probability for carrier scattering, resulting in the significantly suppressed non-radiative decay. Our findings clearly show that the characteristics of STEs in low-dimensional metal halides can be well-tuned by external pressure, and enhanced optical properties can be achieved.

Introduction

Developing light-emitting materials with high photoluminescence quantum yields (PLQYs) is highly demanded for energy saving, considering one-fifth of global electricity is consumed by lighting.[1,2] Most commercial LED white-light sources consisting of multiple emitters encounter the problem of color changing over time, due to the unequal degradation rates of the emitters.[3-5] Single-component materials exhibiting broadband emissions covering the entire visible-light region (spanning 400-800 nm) have the potential to address this problem. However, achieving a broadband emission from a single-component material is not trivial. Recently, molecularly low-dimensional (low-D) metal halides have received wide attention due to their unique optical properties, such as strongly Stokes-shifted broadband emissions.[6-9] Self-trapped excitons (STEs) caused by the strong electron-phonon coupling in low-D metal halides are generally believed to be responsible for the broadband emissions, which significantly depend on the exciton binding energy.[10,11] This suggests that adjusting the lattice and electronic structures using chemical tailoring or external stimuli, such as temperature and pressure, would enable the regulation of the binding energy and modulation of the STE-based emission.

Pressure has been utilized as an effective and clean stimulus to regulate the optoelectronic properties of various types of materials,[12-14] including quantum dots,[15] molecular systems,[16] and metal halides.[17-24] The soft lattices of metal halides render them sensitive to pressure, leading to effective modifications under a mild pressure range.[14,25] Some pressure-induced metastable phases and emergent properties could also be retained to ambient conditions.[13,24,26,27] Despite exciting pressure-enhanced/induced emission results reported in hybrid metal halides, the microscopic origins are not fully understood yet. Various mechanisms have been proposed, but mainly focused on the facilitated radiative recombination route.[17,20,21] It is well known that PL efficiency is highly dependent on the competition between radiative (k_r) and non-radiative (k_{nr}) recombination rates. However, the influences of structural evolution on k_r and k_{nr}, especially k_{nr}, have not been well elucidated in those systems under pressure. Therefore, detailed investigation

and direct experimental support is needed to reveal the underlying mechanisms, which are vital for future materials design and screening. In addition, previously reported studies compared the PL intensities at different conditions, while the quantitative determination of PLQYs under gigapascal pressures has been rarely reported. Thus, a direct quantitative method to determine PLQYs under high pressure is highly desirable.

In this work, using *in situ* structural and optical characterizations, we have systematically investigated the pressure-dependent properties of a one-dimensional (1D) hybrid metal halide $C_4N_2H_{14}PbBr_4$, which consists of $[PbBr_4^{2-}]_\infty$ chains with double-edge sharing $[PbBr_6]$ octahedra (Figure S1). The structure could be considered as an assembly of 1D lead bromide quantum wires surrounded and isolated by organic cations.[28] Previous studies found that $C_4N_2H_{14}PbBr_4$ possesses strong electron-phonon coupling and exhibits a broadband emission with a PLQY of ~ 20%, one of the highest values for 1D hybrid metal halides. As the formation of self-trapped states involves structural relaxation and atomic rearrangement,[29] the configuration and stability of STEs are closely related to the structural variations under pressures. During compression, the PLQY of STE emission was found to increase remarkably from 20% to 90%. With *in situ* high-pressure characterizations, we found that the enhanced emission in $C_4N_2H_{14}PbBr_4$ is mainly attributed to the effective suppression of non-radiative loss, which is directly related to the pressure-tuned STE binding energy and confined motion of organic cations.

Results and Discussion

At ambient conditions, $C_4N_2H_{14}PbBr_4$ exhibits a broadband emission from STEs with a full width at half maximum (FWHM) of 0.8 eV and a large Stokes shift of 0.9 eV. This is in contrast with narrow free-excitonic PL (FWHM ~ 100 meV, Stokes shift ~10 meV) in typical 3D and some layered 2D metal halides.[29] The PL peak centered at 2.3 eV, together with a small peak at around 3.2 eV from the free exciton (Figure S2), whose emission energy is close to the bandgap.[28] During compression, the PL intensity first decreased when the pressure increased from ambient to 1.5 GPa (Figure 1a). Subsequently, the PL intensity increased dramatically with pressure increasing from 1.5 to 2.8 GPa. At 2.8 GPa, the integrated PL intensity was enhanced by over four times compared to the initial value. Meanwhile, the free-exciton emission disappeared (Figure S2). Upon further compression, the PL intensity decreased and blue-shifted, which is caused by a pressure-induced phase transition (we will elaborate on this later). The PL photographs at different pressures clearly demonstrate the change of emission brightness (Figure 1b and Figure S3). Note that the colors across the crystal are not quite homogeneous which is probably due to the existence of deviatoric stresses.[30] Based on the International Commission on Illumination (CIE) chromaticity diagram, the emission color can be tuned by pressure, covering a wide color temperature (Figure 1c). The PL intensity exhibits a linear relationship with the excitation laser power (Figure S4), suggesting that the emission does not originate from the defects but from the self-trapped states.[8] The pressure dependence of the PL emission energy and

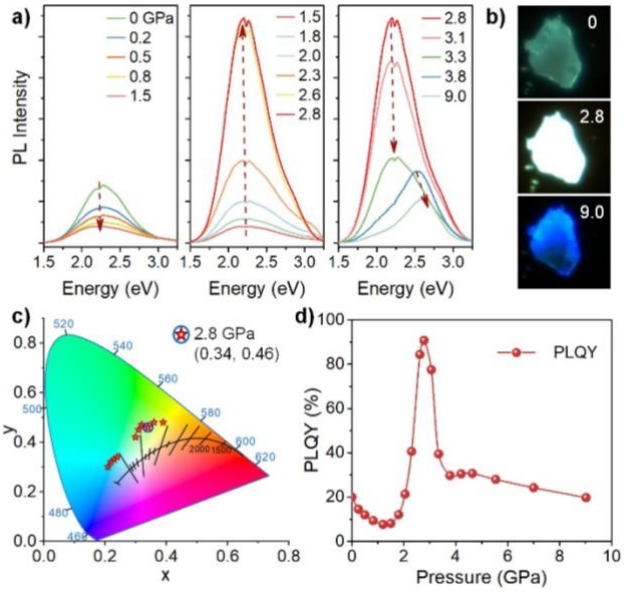

Figure 1. Pressure-dependent PL of $C_4N_2H_{14}PbBr_4$ under 360 nm excitation. a) *In situ* PL spectra at different pressures. b) PL photographs at selected pressures: ambient (top), 2.8 GPa (middle), and 9.0 GPa (bottom). c) Chromaticity coordinates of the emissions under different pressures, showing a wide range of color tunability. d) Evolution of PLQY during compression.

FWHM are provided in Figure S5, which also shows abrupt changes at around 2.8 GPa.

To quantitatively evaluate the emission evolution, PLQY is desired to be determined. To date, PLQY has not been reported in *in situ* gigapascal pressure conditions due to the geometrical unavailability in the integration sphere. By using the PLQY at ambient pressure as a reference, here, we demonstrate a method to estimate PLQY under high pressure from the *in situ* structural and optical results. The PLQY can be calculated using the following formular:[31-33]

$$\Phi = \Phi_R \frac{\int F(\lambda_{\mathrm{em}})}{\int F_{\mathrm{R}}(\lambda_{\mathrm{em}})} \frac{A_R(\lambda_{\mathrm{ex}})}{A(\lambda_{\mathrm{ex}})} \frac{n^2}{{n_{\mathrm{R}}}^2} \quad (1)$$

where Φ is the PLQY, $\int F(\lambda_{\mathrm{em}})$ the integrated intensity of emission, $A(\lambda_{\mathrm{ex}})$ the percentage of light absorbed at the excitation wavelength, n the refractive index, and subscript R denotes the reference data (*i.e.,* the PLQY at ambient pressure). The correction factor ($n^2/{n_{\mathrm{R}}}^2$) was derived from the point source, and the use of this ratio was found to be valid for different detector geometries.[31,34] Detailed methods are described in the Supporting Information. The calculated n and Φ are listed in Table S1 and Figure 1d. At 2.8 GPa, the PLQY of $C_4N_2H_{14}PbBr_4$ increased remarkably to 90%, over four times higher than that at ambient conditions (20%).

The pressure-dependent emission property is closely related to its structural evolution. To unveil the correlation between the optical properties and structure, we characterized the structure variations by *in situ* X-ray diffraction (XRD) and Raman spectroscopy. XRD patterns of $C_4N_2H_{14}PbBr_4$ are shown in Figure 2a. At ambient pressure, the crystal possesses an orthorhombic symmetry of space group *Imma* (74). With increasing pressure, all Bragg

diffraction peaks shifted to larger 2θ. The variations of lattice parameters and unit-cell volume are summarized in Figure S6, indicating anisotropic compressibility where the compression rate along the 1D chain (b axis) is much smaller due to the all-inorganic linking. The compression along the edge-sharing direction (c axis) is smaller than that along the perpendicular direction (a axis) because of the anisotropy of the organic cations. When the pressure reached 2.8 GPa, a set of new peaks appeared abruptly due to symmetry break (Figure S7). Rietveld refinements of the XRD patterns at 2.3 and 2.8 GPa confirmed that the crystal experienced a structural phase transition from the orthorhombic phase (*Imma*) to the monoclinic phase ($P2_1/n$) caused by the sliding of 1D chains along the c axis (Figure 2b). This phase transition can be confirmed by Raman spectroscopy (Figure 2c). Vibrations of the inorganic lead bromide chains of edge-sharing [$PbBr_6$] octahedra are mainly active in low-frequency range (<200 cm^{-1}) due to the large reduced mass, while the vibrational modes of organic cation appear at higher frequency (300-3200 cm^{-1}).[35] Notably, Raman results show that the transformation of the inorganic and organic parts is asynchronous. The vibration mode of organic cations at higher frequency experienced the transition at 2.3 GPa, while the inorganic part stayed at the original vibration mode and changed at a higher pressure (2.9 GPa).

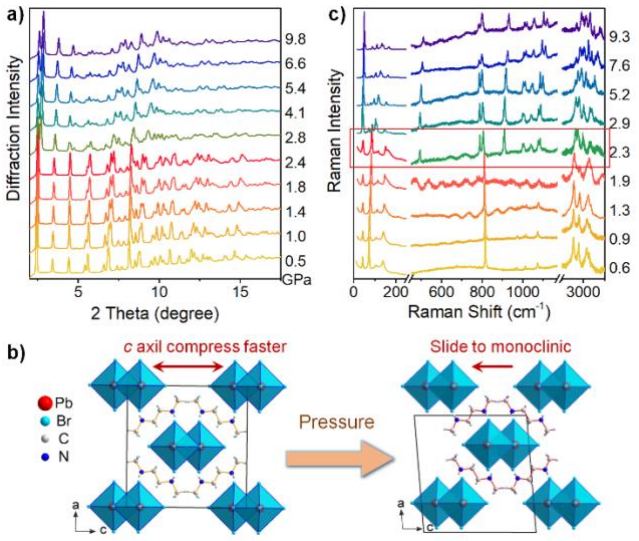

Figure 2. The structural transformation of $C_4N_2H_{14}PbBr_4$ under pressure. a) *In situ* XRD patterns. b) Crystal structure viewing along the 1D chain direction (b axis), illustrating the orthorhombic to monoclinic phase transition at 2.8 GPa. c) Raman spectra.

To elucidate the underlying mechanism of the pressure-enhanced emission, time-resolved PL measurements were conducted to examine the excited state lifetime. The time-resolved PL decays were fitted by double exponential function $I(t) = I(0)\cdot[A_1 \cdot \exp(-t/\tau_1) + A_2 \cdot \exp(-t/\tau_2)]$, and mean PL lifetimes were calculated by $\langle\tau\rangle = [A_1\tau_1^2 + A_2\tau_2^2]/[A_1\tau_1 + A_2\tau_2]$. As Figures 3a, 3b, and 3c depict, the lifetimes did not change much from 0 to 1.9 GPa but sharply increased from 1.9 to 2.8 GPa. At 2.8 GPa, the average lifetime reached over 200 ns, about four times higher than that at ambient conditions. Thereafter, the PL lifetime decreased. The PLQY is determined by the ratio of the radiative recombination rate (k_r) to the sum of radiative and non-radiative (k_{nr}) recombination rates. Either increasing k_r or reducing k_{nr} would increase the PLQY. Based on the PLQY and lifetime (τ) data, one could solve the radiative and non-radiative recombination rate at each pressure using the following equations:[31,36]

$$\mathrm{PLQY} = \frac{k_r}{k_r + k_{nr}} \quad (2)$$

$$\tau = \frac{1}{k_r + k_{nr}} \quad (3)$$

The calculated PLQYs are summarized in Figures 3d & S8 and Table S1. k_{nr} changed dramatically with pressure, while the change of k_r is not significant. We used k^0/k to evaluate the suppression degree for recombination rate under pressure, where k^0 represents the radiative or non-radiative rate at ambient conditions, and k is the rate under pressure. The values of k^0/k below or above 1 indicate the promotion and suppression of recombination, respectively. As shown in Figure 3d and S8, the radiative recombination increased by 18% at around 2.8 GPa. Impressively, at the same time, the non-radiative recombination rate is suppressed by 33 times at 2.8 GPa.

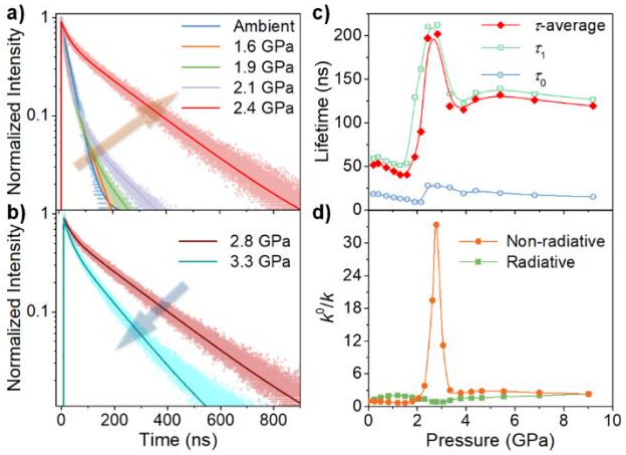

Figure 3. Time-resolved PL of $C_4N_2H_{14}PbBr_4$ under pressure a) 0 to 2.4 GPa; b) 2.8 and 3.3 GPa. c) The PL lifetime as a function of pressure. d) Suppression of radiative and non-radiative recombination rate (k_r^0/k_r and k_{nr}^0/k_{nr}) under high pressure.

Based on the above discussion, the enhanced emission can be elucidated by the vigorously suppressed non-radiative loss as well as the slightly increased radiative recombination rate. Carrier trapping and scattering by defects are the main pathways of non-radiative loss in semiconductors.[37] A high defect density is usually unavoidable in hybrid metal halides due to the wet synthetic method at relatively low temperatures. The efficient PL in the low-D metal halides is believed to be related to the highly localized excitons that reduce the chance to encounter defects.[11] Thermal diffusion and exciton tunneling between inorganic chains are two ways of exciton migration in 1D metal halides. Efficient exciton tunneling requires a resonant condition, *i.e.,* a spectral overlap between exciton excitation and emission.[11] Stokes

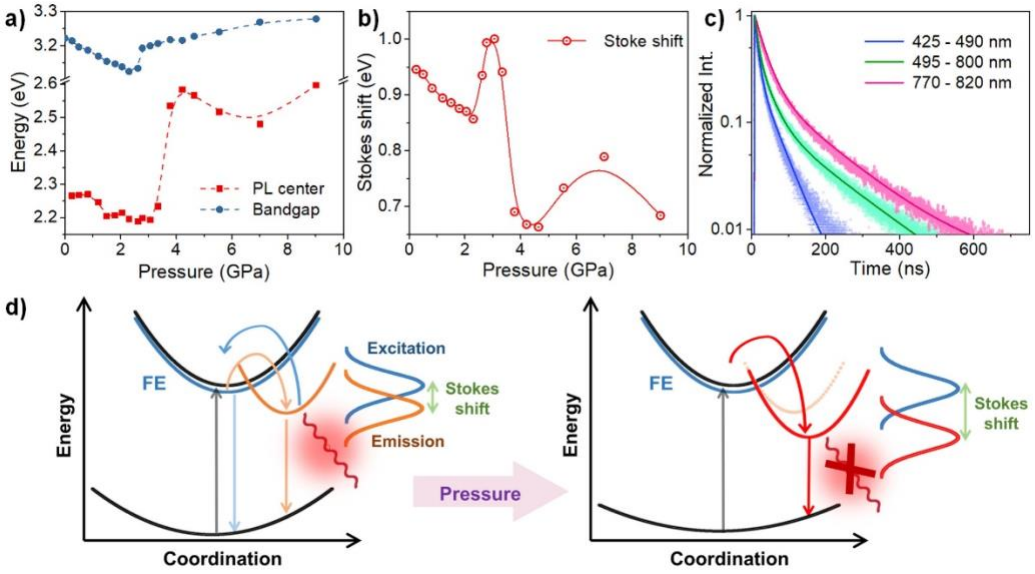

Figure 4. a) Pressure-induced evolution of bandgap and PL emission energy. b) Stokes shift of $C_4N_2H_{14}PbBr_4$ under high pressure. c) Comparison of the PL decay at different wavelength ranges using an optical filter at 2.1 GPa, which implies that the excitons possessing higher binding energy exhibit a longer lifetime and possibly smaller k_{nr}. d) Schematic illustration of the pressure-induced changes in the STE and Stokes shift. STEs would be more stable under a suitable pressure, resulting in a larger Stokes shift and more localized excitons that have less chance to encounter defects. In addition, with increasing STE binding energy, the population of STEs increased while the free exciton (FE) states reduced, as evidenced by the disappearance of the FE emission beyond 2.3 GPa (Figure S2).

shift (E_s) is an indicator to estimate both the spectral overlap and exciton binding energy ($E_{STE\text{-}b} = E_s - E_d$, Figure S9, see detailed information in the Supporting Information), which is directly related to the exciton migration and the non-radiative loss.[38] Figures 4a and 4b show the bandgap, PL emission energy, and the Stokes shift at different pressures. The Stokes shift is calculated from the emission energy and bandgap measured by absorption spectra (Figures S10). The Stokes shift first gradually decreased from ambient to 2.3 GPa, and then sharply increased to over 1 eV at 2.8 GPa, the same trend with PL intensity and lifetime. At 4 GPa, the Stokes shift decreased to below 0.7 eV. The first-principles calculations confirm the evolution behavior of the optical properties (Figure S11 and detailed description in the Supporting Information).

Note that the variation trend of the Stokes shift is in line with that of the non-radiative loss. Stronger excited-state structural relaxation leads to a larger Stokes shift, reaching a suitable level that benefits the STE emission.[10] With larger structural deviation between the ground and excited states, exciton migration from the resonant transfer is also suppressed because of less spectral overlap. This leads to smaller migration of STEs, reducing its chance to encounter defects, which results in the reduced non-radiative loss. The influence of STE binding energy on the PL properties was further investigated by measuring the PL lifetime in different emission wavelength ranges by experimentally adding bandpass optical filters. As shown in Figures 4c and S12, the PL lifetime is longer at the lower energy region, which corresponds to the excitons with higher binding energy and larger Stokes shift. This finding further indicates that the increased STE binding energy of $C_4N_2H_{14}PbBr_4$ during compression is responsible for the longer PL lifetime and lower non-radiative recombination rate, resulting in the enhanced PL performance. Moreover, the increased STE binding energy contributes to the stabilization of STEs. As illustrated in Figure 4d, with increasing STE binding energy, more STEs can be stabilized, and thus, the population of free excitons decreases, as evidenced by the disappearance of the free exciton emission peak at 2.6 GPa (Figure S2).

Aside from defect scattering, the motion of organic cations could also affect non-radiative loss pathway in the perovskites and related low-D metal halides.[39] Previous studies have shown that the halides with more confined and rigid organic cations have brighter emission.[36,37,40] A strategy to "freeze" the organic cations is desirable to suppress non-radiative decay and promote emission properties. In our case, pressure effectively confines and slows down the motion of the $[C_4N_2H_{14}]^{2+}$ cation by squeezing the space between the $[PbBr_6]$ octahedra. As shown in Figure 2c, the blue shift of the Raman peak indicates the hardening of the phonon (vibration) mode. Note that the transitions of the organic and inorganic part of $C_4N_2H_{14}PbBr_4$ are not synchronous. From 2.3 GPa, the vibration modes of the organic cations have already changed, while that of the inorganic skeleton remained unchanged until 2.8 GPa (XRD, which is more sensitive to the inorganic skeleton, also indicates a phase transition after 2.8 GPa). Since the symmetry of the inorganic structural skeleton has not changed at 2.3 GPa, the splitting of the organic cation vibration mode most likely comes from the confinement of molecular motion, making the degenerated mode distinguishable.[41] As a result, the suppressed motion of organic cations effectively reduces the non-radiative recombination[36] at around 2.3 GPa, from where the PL increases dramatically. Further compression leads to a phase transition caused by the sliding of inorganic chains as well as a direct-to-indirect band transition,

indicated by first-principles calculations (Figures S13-14 and detailed information in the Supporting Information). The indirect band structure leads to the deteriorated optical properties after 2.8 GPa. In addition to the pressure-suppressed non-radiative loss, the increased radiative recombination rate by 18% at 2.8 GPa (Figure S8) also contributes to the enhanced PLQY. With the increase of STE binding energy upon compression, more STEs can be stabilized and thus the population of STEs grows. The increasing concentration of localized STEs contributes to the increased k_r.[42]

Conclusion

In conclusion, significant enhancement of the broadband emission in a 1D hybrid metal halide $C_4N_2H_{14}PbBr_4$ was achieved under a mild pressure of 2.8 GPa, where the PLQY was boosted to 90% from the initial value of 20%. A structural phase transition around 2.8 GPa was confirmed by *in situ* XRD and Raman spectroscopy. Time-resolved optical measurements revealed that pressure induced a remarkably suppressed non-radiative loss by 33 times and a promoted radiative recombination rate by 18%, which together contribute to the PL enhancement. Both experimental and computational findings suggest that pressure modulates the STE binding energy and the molecular confinement, resulting in highly localized excitons with reduced scattering by defects and phonons. Our work not only discovers an effective approach to enhancing the PLQY of broadband emission in a 1D metal halide but also provides insights into the microscopic mechanisms that could guide future materials design for highly efficient low-D metal halides for light-emitting applications.

ASSOCIATED CONTENT

Supporting Information. Experimental details, list of pressure dependence of PLQY and recombination rate, fitting of the free exciton peak under low pressure, PL micrograph, Power dependent PL, intensity, FWHM and emission energy of the pressure dependent PL peak, lattice parameters, schematic of the energy level structure of STE, UV-vis absorption spectra, PL decay at different wavelength ranges. refractive index effects in PLQY measurements, and theoretical calculation. This material is available free of charge via the Internet at http://pubs.acs.org.

AUTHOR INFORMATION

Corresponding Author

* xujie.lu@hpstar.ac.cn; bma@fsu.edu; yangwg@hpstar.ac.cn.

Present Addresses

† Department of Physics, University of Washington, Seattle, WA, USA.

‡ Department of Chemistry, The University of Chicago, USA

§ Hoffmann Institute of Advanced Materials, Shenzhen Polytechnic, China

Funding Sources

This work is supported by the National Nature Science Foundation of China (NSFC) (Grant Nos. U1930401, 51527801). C.Z. was supported by the National Science Foundation (DMR-1709116). H.L. and B.M. thank the support from the Air Force Office of Scientific Research under the contract No. FA9550-18-1-0231. M. H. Du was supported by the U. S. Department of Energy, Office of Science, Basic Energy Sciences, Materials Sciences and Engineering Division.

ACKNOWLEDGMENT

This research used resources of the Advanced Photon Source and Center for Nanoscale Materials. They are U.S. Department of Energy (DOE) Office of Science User Facility operated for the DOE Office of Science by Argonne National Laboratory under Contract No. DE-AC02-06CH11357.

REFERENCES

(1) Sun, Y.; Giebink, N. C.; Kanno, H.; Ma, B.; Thompson, M. E.; Forrest, S. R. Management of singlet and triplet excitons for efficient white organic light-emitting devices. *Nature* **2006**, *440*, 908.

(2) Penning, J.; Stober, K.; Taylor, V.; Yamada, M. *Energy savings forecast of solid-state lighting in general illumination applications*, Navigant Consulting Inc., Washington, DC (United States), 2016.

(3) Kitai, A. *Luminescent materials and applications*; John Wiley & Sons, 2008; Vol. 25.

(4) Worku, M.; Xu, L.-J.; Chaaban, M.; Ben-Akacha, A.; Ma, B. Optically pumped white light-emitting diodes based on metal halide perovskites and perovskite-related materials. *APL Mater.* **2020**, *8*, 010902.

(5) Ye, S.; Xiao, F.; Pan, Y.; Ma, Y.; Zhang, Q. Phosphors in phosphor-converted white light-emitting diodes: Recent advances in materials, techniques and properties. *Mater. Sci. Eng., R* **2010**, *71*, 1.

(6) Smith, M. D.; Karunadasa, H. I. White-light emission from layered halide perovskites. *Acc. Chem. Res.* **2018**, *51*, 619.

(7) Lin, H.; Zhou, C.; Tian, Y.; Siegrist, T.; Ma, B. Low-dimensional organometal halide perovskites. *ACS Energy Lett.* **2017**, *3*, 54.

(8) Luo, J.; Wang, X.; Li, S.; Liu, J.; Guo, Y.; Niu, G.; Yao, L.; Fu, Y.; Gao, L.; Dong, Q.; Zhao, C.; Leng, M.; Ma, F.; Liang, W.; Wang, L.; Jin, S.; Han, J.; Zhang, L.; Etheridge, J.; Wang, J.; Yan, Y.; Sargent, E. H.; Tang, J. Efficient and stable emission of warm-white light from lead-free halide double perovskites. *Nature* **2018**, *563*, 541.

(9) Cortecchia, D.; Yin, J.; Petrozza, A.; Soci, C. White light emission in low-dimensional perovskites. *J. Mater. Chem. C* **2019**, *7*, 4956.

(10) de Jong, M.; Seijo, L.; Meijerink, A.; Rabouw, F. T. Resolving the ambiguity in the relation between Stokes shift and Huang–Rhys parameter. *Phys. Chem. Chem. Phys.* **2015**, *17*, 16959.

(11) Han, D.; Shi, H.; Ming, W.; Zhou, C.; Ma, B.; Saparov, B.; Ma, Y.-Z.; Chen, S.; Du, M.-H. Unraveling luminescence mechanisms in zero-dimensional halide perovskites. *J. Mater. Chem. C* **2018**, *6*, 6398.

(12) Mao, H.-k.; Mao, W. L. Key problems of the four-dimensional Earth system. *Matter Radiat. Extremes* **2020**, *5*, 038102.

(13) Bai, F.; Bian, K.; Huang, X.; Wang, Z.; Fan, H. Pressure Induced Nanoparticle Phase Behavior, Property, and Applications. *Chem. Rev.* **2019**, *119*, 7673.

(14) Zhang, L.; Wang, K.; Lin, Y.; Zou, B. Pressure Effects on the Electronic and Optical Properties in Low-Dimensional Metal Halide Perovskites. *J. Phys. Chem. Lett.* **2020**, *11*, 4693.

(15) Xiao, G.; Wang, Y.; Han, D.; Li, K.; Feng, X.; Lv, P.; Wang, K.; Liu, L.; Redfern, S. A.; Zou, B. Pressure-Induced Large Emission Enhancements of Cadmium Selenide Nanocrystals. *J. Am. Chem. Soc.* **2018**, *140*, 13970.

(16) Zhang, S.; Dai, Y.; Luo, S.; Gao, Y.; Gao, N.; Wang, K.; Zou, B.; Yang, B.; Ma, Y. Rehybridization of nitrogen atom induced photoluminescence enhancement under pressure stimulation. *Adv. Funct. Mater.* **2017**, *27*, 1602276.

(17) Li, Q.; Chen, Z.; Yang, B.; Tan, L.; Xu, B.; Han, J.; Zhao, Y.; Tang, J.; Quan, Z. Pressure-Induced Remarkable Enhancement of Self-Trapped Exciton Emission in One-Dimensional CsCu2I3 with Tetrahedral Units. *J. Am. Chem. Soc.* **2020**, *142*, 1786.

(18) Castelli, A.; Biffi, G.; Ceseracciu, L.; Spirito, D.; Prato, M.; Altamura, D.; Giannini, C.; Artyukhin, S.; Krahne, R.; Manna, L. Revealing Photoluminescence Modulation from Layered Halide Perovskite Microcrystals upon Cyclic Compression. *Adv. Mater.* **2019**, *31*, 1805608.

(19) Zhang, L.; Liu, C.; Wang, L.; Liu, C.; Wang, K.; Zou, B. Pressure-Induced Emission Enhancement, Band-Gap Narrowing, and Metallization of Halide Perovskite Cs3Bi2I9. *Angew. Chem., Int. Ed.* **2018**, *57*, 11213.

(20) Ma, Z.; Liu, Z.; Lu, S.; Wang, L.; Feng, X.; Yang, D.; Wang, K.; Xiao, G.; Zhang, L.; Redfern, S. A. T.; Zou, B. Pressure-induced emission of cesium lead halide perovskite nanocrystals. *Nat. Commun.* **2018**, *9*, 4506.

(21) Shi, Y.; Ma, Z.; Zhao, D.; Chen, Y.; Cao, Y.; Wang, K.; Xiao, G.; Zou, B. Pressure-Induced Emission (PIE) of One-Dimensional Organic Tin Bromide Perovskites. *J. Am. Chem. Soc.* **2019**, *141*, 6504.

(22) Li, M.; Liu, T.; Wang, Y.; Yang, W.; Lü, X. Pressure responses of halide perovskites with various compositions, dimensionalities, and morphologies. *Matter Radiat. Extremes* **2020**, *5*, 018201.

(23) Wang, T.; Daiber, B.; Frost, J. M.; Mann, S. A.; Garnett, E. C.; Walsh, A.; Ehrler, B. Indirect to direct bandgap transition in methylammonium lead halide perovskite. *Energy Environ. Sci.* **2017**, *10*, 509.

(24) Guo, S.; Zhao, Y.; Bu, K.; Fu, Y.; Luo, H.; Chen, M.; Hautzinger, M. P.; Wang, Y.; Jin, S.; Yang, W.; Lü, X. Pressure-Suppressed Carrier Trapping Leads to Enhanced Emission in Two-Dimensional Perovskite (HA)2(GA)Pb2I7. *Angew. Chem., Int. Ed.* **2020**, doi.org/10.1002/ange.202001635

(25) Cao, Y.; Qi, G.; Sui, L.; Shi, Y.; Geng, T.; Zhao, D.; Wang, K.; Yuan, K.; Wu, G.; Xiao, G.; Lu, S.; Zou, B. Pressure-Induced Emission Enhancements of Mn2+-Doped Cesium Lead Chloride Perovskite Nanocrystals. *ACS Mater. Lett.* **2020**, *2*, 381.

(26) Kong, L.; Liu, G.; Gong, J.; Mao, L.; Chen, M.; Hu, Q.; Lü, X.; Yang, W.; Kanatzidis, M. G.; Mao, H.-k. Highly tunable properties in pressure-treated two-dimensional Dion–Jacobson perovskites. *Proc. Natl. Acad. Sci. U. S. A.* **2020**, *117*, 16121.

(27) Lü, X.; Wang, Y.; Stoumpos, C. C.; Hu, Q.; Guo, X.; Chen, H.; Yang, L.; Smith, J. S.; Yang, W.; Zhao, Y.; Xu, H.; Kanatzidis, M. G.; Jia, Q. Enhanced Structural Stability and Photo Responsiveness of CH3NH3SnI3 Perovskite via Pressure-Induced Amorphization and Recrystallization. *Adv. Mater.* **2016**, *28*, 8663.

(28) Yuan, Z.; Zhou, C.; Tian, Y.; Shu, Y.; Messier, J.; Wang, J. C.; Van De Burgt, L. J.; Kountouriotis, K.; Xin, Y.; Holt, E. One-dimensional organic lead halide perovskites with efficient bluish white-light emission. *Nat. Commun.* **2017**, *8*, 14051.

(29) Smith, M. D.; Connor, B. A.; Karunadasa, H. I. Tuning the luminescence of layered halide perovskites. *Chem. Rev.* **2019**, *119*, 3104.

(30) Wang, Z.; Schliehe, C.; Wang, T.; Nagaoka, Y.; Cao, Y. C.; Bassett, W. A.; Wu, H.; Fan, H.; Weller, H. Deviatoric Stress Driven Formation of Large Single-Crystal PbS Nanosheet from Nanoparticles and in Situ Monitoring of Oriented Attachment. *J. Am. Chem. Soc.* **2011**, *133*, 14484.

(31) Lakowicz, J. R. *Principles of Fluorescence Spectroscopy*; 3rd ed.; Springer, 2006.

(32) Demas, J. N.; Crosby, G. A. Measurement of photoluminescence quantum yields. Review. *J. Phys. Chem.* **1971**, *75*, 991.

(33) Rurack, K.; Spieles, M. Fluorescence quantum yields of a series of red and near-infrared dyes emitting at 600− 1000 nm. *Anal. Chem.* **2011**, *83*, 1232.

(34) Hermans, J.; Levinson, S. Some geometrical factors in light-scattering apparatus. *J. Opt. Soc. Am.* **1951**, *41*, 460.

(35) Niemann, R. G.; Kontos, A. G.; Palles, D.; Kamitsos, E. I.; Kaltzoglou, A.; Brivio, F.; Falaras, P.; Cameron, P. J. Halogen effects on ordering and bonding of CH3NH3+ in CH3NH3PbX3 (X= Cl, Br, I) hybrid perovskites: a vibrational spectroscopic study. *J. Phys. Chem. C* **2016**, *120*, 2509.

(36) Gong, X.; Voznyy, O.; Jain, A.; Liu, W.; Sabatini, R.; Piontkowski, Z.; alters, G.; Bappi, G.; Nokhrin, S.; Bushuyev, O. Electron–phonon interaction in efficient perovskite blue emitters. *Nat. Mater.* **2018**, *17*, 550.

(37) Luo, D.; Su, R.; Zhang, W.; Gong, Q.; Zhu, R. Minimizing non-radiative recombination losses in perovskite solar cells. *Nat. Rev. Mater.* **2019**, 1.

(38) Dean, P.; Herbert, D. In *Excitons*; Springer: 1979, p 55.

(39) Gautier, R.; Massuyeau, F.; Galnon, G.; Paris, M. Lead Halide Post-Perovskite-Type Chains for High-Efficiency White-Light Emission. *Adv. Mater.* **2019**, *31*, 1807383.

(40) Wright, A. D.; Verdi, C.; Milot, R. L.; Eperon, G. E.; Pérez-Osorio, M. A.; Snaith, H. J.; Giustino, F.; Johnston, M. B.; Herz, L. M. Electron–phonon coupling in hybrid lead halide perovskites. *Nat. Commun.* **2016**, *7*, 11755.

(41) Ferraro, J. R. *Introductory raman spectroscopy*; Elsevier, 2003.

(42) deQuilettes, D. W.; Frohna, K.; Emin, D.; Kirchartz, T.; Bulovic, V.; Ginger, D. S.; Stranks, S. D. Charge-Carrier Recombination in Halide Perovskites. *Chem. Rev.* **2019**, *119*, 11007.